Journal of Structural Geology 37 (2012) 150–160

Contents lists available at SciVerse ScienceDirect

Journal of Structural Geology

journal homepage: www.elsevier.com/locate/jsg

Shearing of magma along a high-grade shear zone: Evolution of microstructures during the transition from magmatic to solid-state flow

I. Zibra [a,*], J.H. Kruhl [b], A. Montanini [c], R. Tribuzio [d]

[a] Geological Survey of Western Australia, 100 Plain Street, East Perth, Western Australia 6004, Australia
[b] Tectonics and Material Fabrics Section, Faculty of Civil and Geodetic Engineering, Technische Universität München, Arcisstraße 21, 80290 Munich, Germany
[c] Dipartimento di Scienze della Terra, Universita' di Parma, Parco Area delle Scienze 157a, 43100 Parma, Italy
[d] Dipartimento di Scienze della Terra, Universita' di Pavia, Via Ferrata 1 27100 Pavia, Italy

ARTICLE INFO

Article history:
Received 9 August 2011
Received in revised form
22 December 2011
Accepted 20 January 2012
Available online 31 January 2012

Keywords:
Crustal-scale shear zone
Syntectonic granite
Quartz <c>
Axis fabrics
SynMagmatic deformation
Microfabric

ABSTRACT

Syntectonic plutons may record short-lived geological events related to crustal melting and deformation of the continental crust. Therefore, interpretation of microstructure and orientation of fabrics is critical in order to constrain space/time/temperature/deformation relationships during pluton crystallization. Here we describe the transition from magmatic to solid-state deformation in the late-Variscan Diorite-Granite Suite (DGS) emplaced along the Santa Lucia Shear Zone. The systematic collection of meso-, microstructural and quartz < c > axis data allow us to examine the spatial distribution and the mode of superposition of different fabrics. We identify three magmatic microfabric types, thought to reflect the microstructural evolution at decreasing melt content during pluton crystallization. Our data suggest that diffusion creep, dislocation creep and grain-scale fracturing cooperated in accommodating the shearing of the partially molten quartzofeldspathic aggregate. We suggest that the switch from upward to horizontal magmatic flow occurred at melt fractions gt; ~0.40, and that most of the hypersolidus fabrics formed during horizontal flow, reflecting the stress field imposed by the shear zone, and preserving no memory of the ascent stage.

1. Introduction

The establishment of a causal link between shear zones activity and pluton emplacement should be evaluated carefully, since it requires the verification of a spatial, geometrical and temporal correlation, together with comparable rates of shear zone movement and magma supply (Paterson and Tobisch, 1992; Paterson and Schmidt, 1999). Within the available literature regarding syntectonic plutons these requirements are not always matched. However, a relationship between shear zones and pluton emplacement has been fully documented in a number of cases (Rosenberg, 2004, for a review). Magma ascent may occur along pre-existing shear zones, and shear zones may nucleate within thermally softened, partially molten crustal domains (Neves et al., 1996). Since emplacement, crystallization and cooling of syntectonic plutons may represent relatively rapid geological processes (Paterson and Tobisch, 1992; Karlstrom et al., 1993; Bodorkos et al., 2000; Petford et al., 2000), granite plutons may record short-lived geological events related to crustal melting and deformation of the continental crust. Different portions of a pluton may record different fabrics, reflecting subsequent stages of syndeformational crystallization. Therefore, interpretation of microstructure and orientation and intensity of fabrics is critical in order to constrain space/time/temperature/deformation relationships during pluton crystallization. Multiple criteria need to be addressed to fully document the syntectonic character of granitoid plutons, including (i) parallelism between magmatic fabric in the pluton and solid-state fabric in the adjacent country rocks (Paterson et al., 1998); (ii) consistency of shear sense across pluton boundaries (Blumenfeld and Bouchez, 1988); (iii) evidence of melt-present deformation, to document the continuity of deformation from hypersolidus to subsolidus conditions. Although deformed granitic plutons exposed near shear zones are often considered syntectonic, such a transition has been rarely fully documented (e.g. Miller and Paterson, 1994; Büttner, 1999). Over the past twenty years, significant progress has been made in understanding the microstructural evolution of crystallizing or melting rocks, and several meso- and microstructural criteria are thus available to distinguish between

* Corresponding author. Tel.: +61 8 9222 3082; fax: +61 8 9222 3633.
E-mail addresses: ivan.zibra@dmp.wa.gov.au (I. Zibra), kruhl@tum.de (J.H. Kruhl), alessandra.montanini@unipr.it (A. Montanini), tribuzio@crystal.unipv.it (R. Tribuzio).

0191-8141/$ – see front matter Crown Copyright © 2012 Published by Elsevier Ltd. All rights reserved.
doi:10.1016/j.jsg.2012.01.011

magmatic and solid-state deformation (Vernon, 2000 for a review). Nevertheless, criteria to identify flow at low melt fraction are still debated, because microstructures developed at that stage could be similar to those acquired during high-temperature solid-state flow. Also, these transient microstructures are generally poorly preserved in nature, mainly because of subsequent annealing and/or solid-state overprint (Rosenberg, 2001).

In this paper we describe the transition from magmatic to solid-state deformation in the late-Variscan Diorite-Granite Suite (DGS) emplaced along the Santa Lucia Shear Zone (SLSZ, Zibra et al., 2010). The systematic collection of meso-, microstructural and quartz < c > axis (i.e. about 100 thin section were studied) allow us to examine the spatial distribution and the modality of superposition of different fabrics. Moreover, we discuss the evolution of microstructures thought to reflect the progressive syndeformational crystallization and cooling and we speculate on different deformation mechanisms that could have been prevailing during the shearing of the quartzofeldspathic aggregate. This study emphasizes the importance of quartz < c > and microstructure investigation for the recognition of different deformation stages developed under a consistent kinematic framework.

2. Geological setting

In the Western Mediterranean, Corsica is located between two Tertiary back-arc basins (Doglioni et al., 1997) and is divided into two structural domains: in the west, the Variscan domain is mainly composed of granitoid rocks emplaced during the late- to post-collisional phases of the Variscan orogeny (Paquette et al., 2003). The Alpine Corsica is a stack of nappes of Alpine age, derived either from oceanic protoliths (ophiolites) or continental basement (Egal, 1992; Caron, 1994). In this context, the S. Lucia basement represents a fragment of the late-Variscan lower crust (Rossi et al., 2005), covered by Cretaceous sedimentary rocks (Fig. 1). This basement-cover sequence recorded a polyphase Alpine tectonic evolution, mainly developed under lower greenschist facies conditions (Zibra, 2006).

Within the Santa Lucia basement, three complexes have been identified by lithological and structural criteria (Fig. 1). The easternmost complex consists of a fragment of a km-thick shear zone (the S. Lucia Shear Zone, SLSZ) mainly made up of Permian metagabbros. The SLSZ recorded a granulite-facies metamorphic peak dated at 286 ± 1 Ma (Paquette et al., 2003), followed by a main shear event accompanied by isothermal decompression from ~7 to 5 kbar at ~800 °C (Zibra et al., 2010). The Diorite-Granite Suite, DGS (Fig. 1) consists of a magmatic suite of gabbro-dioritic to granitic composition, which has been interpreted as cogenetic with the gabbroic protolith of the SLSZ (Libourel, 1985); the DGS suite was emplaced during the latest stages of shearing recorded by the SLSZ (280 ± 2 Ma, Paquette et al., 2003). In the SW, the Leucogranitic Complex (LGC) mainly consists of undated Hbl- to Bt-bearing tonalites and of two-mica microgranitoids.

The DGS is composed of four main granitoid units, displaying a compositional zoning roughly concordant with the SLSZ (Fig. 1). In the northernmost area, the coarse-grained Opx-bearing tonalite grades westward into an amphibole-rich unit characterized by a millimetre- to metre-scale diorite-tonalite layering (Fig. 4a in Zibra et al., 2010). Tonalite-diorite is intruded by coarse-grained porphyritic granite, locally displaying *rapakivi* texture, and then by leucogranite, which mainly occurs as dykes of various sizes.

Magmatic foliation and lineation are defined by aligned euhedral feldspar and amphibole phenocrysts and commonly overprints both igneous contacts (Fig. 2.53 and 2.56 – Zibra, 2006) and map-scale compositional changes (see the trace of magmatic foliation, Fig. 1). It is cut by late-stage pegmatites and aplites, indicating that the foliation developed after the intrusion of most of the granitoid\mafic rocks, but before the full crystallization of the pluton (Paterson et al., 1998). The magmatic foliation is deformed by a 10–50 m spaced network of anastomosing, high-temperature shear zones, ranging from a few cm to a few m in thickness (Zibra, 2006; p.67); they can usually be traced for a few tens of metres along strike and commonly exhibit diffuse boundaries against wall rocks. In the southern area, these shear zones are more closely spaced, and the solid-state overprint is nearly complete. The NW-SE subvertical mylonitic foliation bears a SE plunging stretching lineation marked by quartz ribbons and elongate trails of feldspars, hornblende and biotite.

3. P-T conditions of emplacement

We have applied conventional thermobarometry to mineral phases of magmatic origin, in order to constrain P-T conditions prevailing during DGS emplacement. Mineral analyses were carried out at the Earth Sciences Department of Parma University with a JEOL-6400 electron microprobe equipped with LINK-ISIS energy-dispersive microanalytic system. Operating conditions were accelerating voltage of 15 kV and probe current of 0.25 nA, a spot diameter of 1–2 μ and counting time of 100 s. Both natural minerals and synthetic compounds were used as standards. Selected amphibole and plagioclase analyses are reported in Table 1, whereas amphibole classification according to Leake (1997) is shown in Fig. 2. The amphibole composition varies from edenite-ferroedenite to ferropargasite, ferrotschermakite and magnesio-hornblende with decreasing A-site occupancy. TiO_2 contents range between 1.4 and 2.2 wt%. No significant compositional zoning from core to rim was detected.

Pressure estimates have been obtained using the "Al in Hbl" barometer, which is based on the assumption that the Al content in hornblende increases with pressure. Since the barometer is also temperature-dependent (Anderson and Smith, 1995), the most recent calibration from these authors has been adopted in this work. The barometer fails to yield high pressure values for low-f_{O2} plutons with iron-rich hornblende (Anderson and Smith, 1995). Therefore, this calibration has been used here only when $Fe_{tot}/(Fe_{tot} + Mg)$ ratios of hornblende are in the range ~0.40–0.65, indicating relatively high f_{O2}, as recommended by these authors. Furthermore, only plagioclase showing An content in the range An25–An35 are used here, because higher anorthite content can markedly increase the Al content in Hbl, independently of pressure (Anderson and Smith, 1995). In the DGS, most granitoids display K-feldspar-free tonalitic composition or, when K-feldspar is present, they lack hornblende. Although the absence of K-feldspar and titanite generally does not produce any detectable error in the calculated pressure (Anderson and Smith, 1995), pressure estimations obtained from tonalites have to be considered as maximum values (Anderson, 1996).

Temperature conditions of the tonalite crystallization have been calculated applying the edenite-richterite revised calibration of the amphibole-plagioclase thermometer (Holland and Blundy, 1994). Pressure and temperature constraints, provided by hornblende and plagioclase crystals with appropriate composition, are summarized in Table 2.

The obtained temperatures likely record a near-solidus stage for tonalite compositions at the estimated pressure, according to the experimental curves of Singh and Johannes (1996) reported in Fig. 3. Comparison with other experimental works on similar systems (Fig. 3) suggests that the hornblende-plagioclase temperatures may also reflect some cooling below their magmatic crystallization as a consequence of a slow cooling rate of the plutonic body. The shaded box representing the P-T estimates for DGS

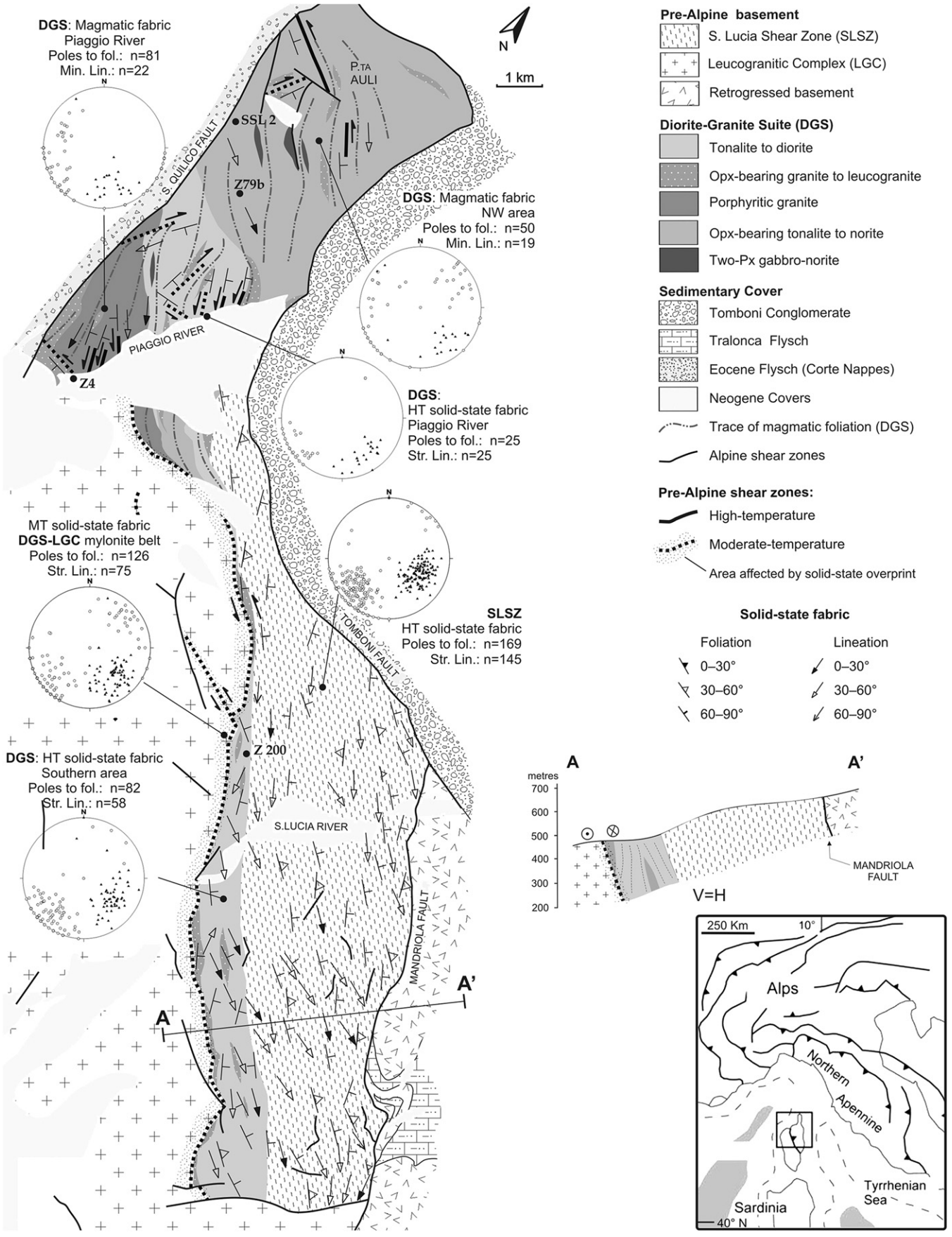

Fig. 1. Geological map and cross section of the S. Lucia basement, with the insets of equal area projection plots (lower hemisphere) of mineral and stretching lineation (black triangles) and poles to foliation (open circles). The location of the four samples selected for PT estimation is shown.

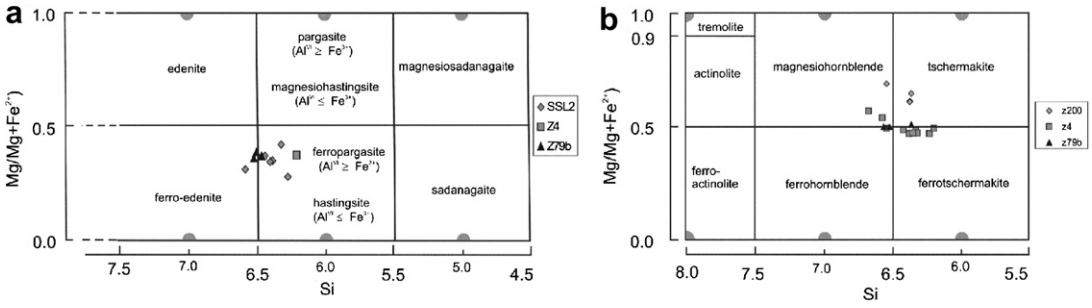

Fig. 2. Variations of Mg/(Mg + Fe2+) vs. Si (apfu) for the DGS magmatic amphiboles and classification of calcic amphiboles (Leake, 1997) with (Na + K) A < 0.5 (a) and gt; 0.5 (b), respectively.

emplacement (Fig.3) takes also into account the microstructural constraints described below, i.e. quartz deformation occurred in the high-quartz field during pluton crystallization.

4. Microstructures

4.1. Magmatic fabric

Within the domains characterized by magmatic foliation, three main microfabric types have been identified by microstructural criteria, from samples with comparable assemblage (leucotonalite to leucogranite) and average grain size (~10 mm). Field relations and microstructures suggest that a gradual transition occurs between the main microfabric types.

In microfabric type (I), aligned tabular feldspars, amphibole and pyroxene that are not internally deformed and display euhedral faces are surrounded by anhedral, undeformed quartz grains or non-aligned quartz aggregates (Fig. 4a). Thus, this microfabric reflects magmatic flow with limited grain-to-grain interactions and subsequent crystallization under static conditions (Hutton, 1988; Rosenberg, 2001).

Microfabric type (II) is defined by the onset of plastic deformation in quartz that occurs as mono- to polycrystalline lenses (aspect ratios of up to 5:1, Fig. 4b), with a prominent shape preferred orientation (SPO) parallel to the magmatic foliation.

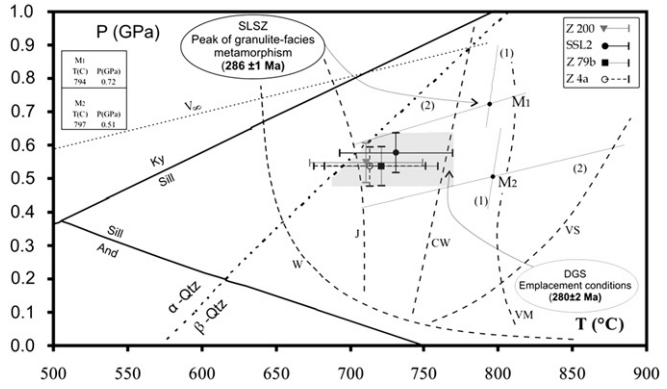

Fig. 3. P-T conditions for DGS emplacement and for M_1 and M_2 assemblages in the SLSZ (modified from Zibra et al., 2010). Al_2SiO_5 phase relations are calculated using winTWQ (v. 2.32). The α-/β- quartz transition is from Gross and Van Heege (1973). Equilibrium (1) is the geothermometer Alm + Phl = Prp + Ann; equilibrium (2) is the geobarometer 2 Alm + Grs + 3 βQtz = 6Fs + 3 An. The emplacement age of DGS results from the mean of two sample ages (U–Pb zircon ages, Paquette et al., 2003). J: solidus for the tonalite system (biotite-plagioclase-quartz) from Johannes (1984); other fluid-absent solidi for granitoid systems are taken from Clemens and Wall (1981): CW; Vielzeuf and Montel (1994): VM; Vielzeuf and Schmidt (2001): VS. W = H_2O–saturated haplogranite solidus (Singh and Johannes, 1996).

Quartz grains commonly show chessboard subgrain boundary (SGB) pattern (fig.2.59, Zibra, 2006). Polycrystalline aggregates show mosaic-like grain boundary patterns, coarsely lobate grain boundaries and a wide range of grain size (~50–1000 μm). Therefore, quartz shows evidence of intracrystalline plasticity, where recrystallization occurred by dominant grain boundary migration (GBM; Stipp et al., 2002) in the high-quartz field ($T \geq$ ~700°, Fig. 3; see also Kruhl, 1996).

The onset of widespread plastic deformation in feldspar defines microfabric type (III). Here, both plagioclase and K-feldspar show sweeping undulose extinction and widespread recrystallization. The margins of the porphyroclasts contain subgrains with lobate outlines and sizes similar to that of the recrystallized grains (~200–500 μm, Fig. 4c and d), indicating that crystal-plastic deformation in the dislocation creep regime was active in feldspars (Ji and Mainprice, 1990) and that recrystallization is likely to have occurred by dominant subgrain rotation (Rosenberg and Stünitz, 2003). In both feldspar porphyroclasts and recrystallized grains, quartz-feldspar phase boundaries are commonly coarsely lobate, with phase boundary cusps consistently pointing along the foliation trace (Fig. 4d). This morphology reflects phase boundary migration assisted by diffusion creep at temperatures above ~650° (Gower and Simpson, 1992; Rosenberg and Stünitz, 2003), which was active during and/or after feldspar recrystallization.

Grain-scale brittle feldspars deformation is common in samples displaying microfabric (II) and (III). Intragranular fractures typically affect a single grain and are sealed by quartz, optically continuous with the adjacent matrix quartz (Fig. 4e). Composite plagioclase-quartz infill may also occur (Fig. 4f). The An content in plagioclase of ~10% (estimated by conventional optical methods) suggests that this microstructure represents magmatic microfractures sealed by a melt that evolved towards a residual composition (Bouchez et al., 1992; John and Stünitz, 1997). In sample z5 (Fig. 4c–f), thin magmatic microfractures have relatively straight walls and transect lobate quartz-feldspar phase boundaries (arrow head in Fig. 4d).

Given the estimated pressure of emplacement (Fig.3), the occurrence of chessboard SGB pattern in quartz from microfabric (II) and (III) indicates deformation in the high-quartz field (Kruhl, 1996), at about 700 ± 30 °C, in agreement with the crystallization temperature provided by the Hbl-Pl thermometer (720 ± 40 °C).

4.2. High-temperature solid-state fabric

In the shear zones, quartz occurs as polycrystalline ribbons made up of recrystallized coarse grains, alternating with quartz-free layers composed of partially to totally recrystallized feldspars (Fig. 5; see also Figs. 2.71 to 2.76 in Zibra, 2006). K-feldspar porphyroclasts display sweeping undulose extinction and core-and-mantle microstructure. Near the margin of porphyroclasts, the

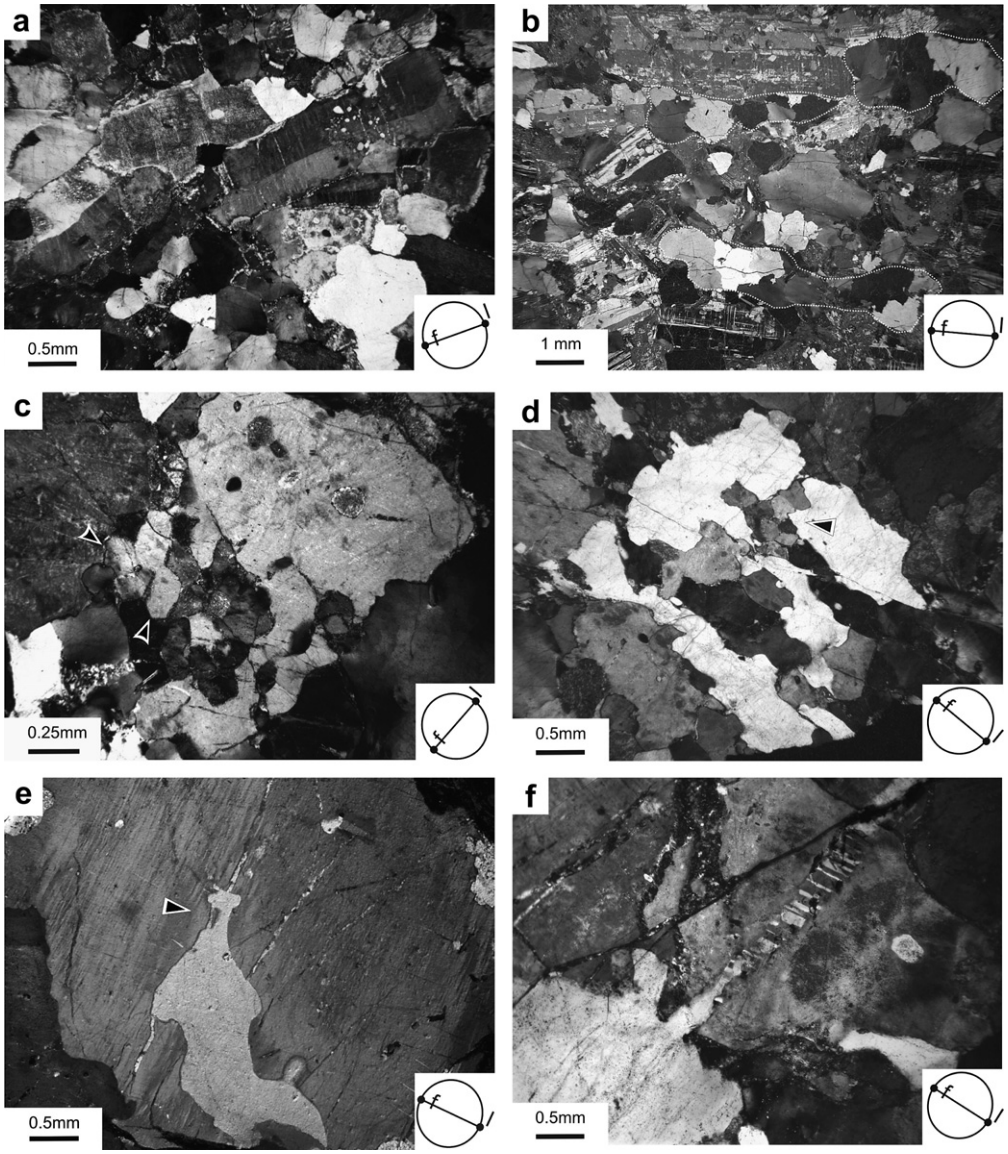

Fig. 4. Magmatic microfabrics; crossed polars; inset field of view with respect to lineation (l) and foliation (f). Figs. 4c–f are from the same sample (z5). (a) Type (I) microfabric, with aligned tabular K-feldspar and plagioclase (partly altered). Interstitial quartz does not exhibit any visible shape fabric or internal deformation features (sample DSL60). (b) Microfabric type (II), showing quartz aggregates (highlighted by white dashed lines) elongate parallel to the primary foliation. Coarsely sutured quartz grain boundaries suggest weak deformation at relatively high-temperatures. (c) K-feldspar porphyroclast partially replaced by recrystallized grains of 100–200 μ in diameter. Porphyroclast margins contain subgrains (indicated by arrowheads) of comparable size. Trails of thin quartz recrystallized grains (lower left) are related to a moderate low-temperature overprint. (d) Typical type (III) microfabric, with cuspate and lobate phase boundaries between quartz (white) and K-feldspar porphyroclasts and recrystallized grains (arrow head), where cusps consistently point along the foliation trace. (e) Lobate phase boundary between quartz and K-feldspar. Arrow head points to a Kfs promontory truncated by a quartz-filled magmatic microfracture (f) A magmatic microfracture in K-feldspar with quartz-albite Composite infill and albite growth twins.

observed gradual transition between subgrains and new grains (arrows in Fig. 5) suggests feldspar recrystallization by dominant subgrain rotation at Tgt; ~600 °C (Rosenberg and Stünitz, 2003). In the sheared melanocratic granitoids, poikilitic hornblende porphyroblasts include the recrystallized quartz-plagioclase mylonitic matrix, and orthopyroxene porphyroclasts are rimmed by hornblende-quartz symplectites (Zibra, 2006) indicating amphibolite-facies conditions.

5. Quartz crystallographic preferred orientation

5.1. Magmatic fabric

The activation of particular slip systems and the development of crystallographic preferred orientation (CPO) are largely a function of temperature, strain rate and deformation regime (Passchier and Trouw, 2005 and references therein). In this paper, we use quartz CPO data collected by conventional U-stage techniques to obtain information about the dominant deformation mechanisms, and to constrain shear sense and temperature of deformation, through a comparison with data obtained from thermobarometry. 300 measurements are generally thought to provide a reliable representation of quartz fabrics of medium intensity. However, six of our samples contain fewer large, non-recrystallized grains (Fig. 6). Therefore, results from these samples should be considered with some caution.

In microfabric type (I) (sample DSL60, Fig. 4a), the c-axis pattern displays a nearly complete girdle along the foliation plane (XY plane), with two prominent maxima close to the magmatic lineation (i.e. the near-X maxima), joined with a secondary near-Y

Table 1
Representative plagioclase–amphibole pairs in selected DGS granitoids.

Sample	Z200			SSL2			Z4			Z79B		
Rock type mineral	Pl	Amph		Pl	Amph		Pl	Amph		Pl	Amph	
		Tsch *c*	Tsch *r*		Ed *c*	Fe-Prg *r*		Fe-Tsch *c*	Fe-Tsch *r*		Fe-ed *c*	Fe-Prg *r*
SiO2	57.69	43.22	42.29	58.09	42.50	40.93	60.00	42.19	42.90	59.80	42.65	42.19
TiO2	0.00	1.79	1.71	0.03	2.21	1.94	0.05	1.46	1.62	0.04	2.19	1.89
Al2O3	25.52	11.35	11.05	24.93	10.23	11.42	25.24	11.23	10.63	24.94	10.71	10.96
FeO	0.21	17.20	16.81	0.86	20.46	20.09	0.00	20.71	20.40	0.11	18.91	19.21
MnO	0.00	0.42	0.38	0.08	0.32	0.27	0.00	0.79	0.81	0.04	0.52	0.47
MgO	0.00	10.31	10.20	0.11	6.96	7.10	0.32	7.62	8.26	0.00	7.96	8.00
CaO	8.22	11.22	11.21	7.66	11.35	10.77	7.05	11.30	11.71	6.89	10.97	11.13
Na2O	6.35	1.28	1.17	6.72	0.98	1.13	7.86	0.99	0.96	7.77	1.82	1.85
K2O	0.55	1.36	1.34	0.54	1.89	2.13	–	1.29	1.28	0.30	1.80	1.72
Total	98.54	98.15	96.16	99.02	96.90	95.78	100.52	97.58	98.57	99.89	97.53	97.42
Si	2.620	6.381	6.379	2.636	6.579	6.375	2.660	6.387	6.432	2.670	6.520	6.459
Ti	0.000	0.199	0.194	0.000	0.257	0.227	0.000	0.166	0.183	0.000	0.252	0.218
Altot	1.370	1.975	1.964	1.332	1.866	2.096	1.320	2.003	1.878	1.310	1.930	1.977
AlIV	–	1.619	1.621	–	1.421	1.625	–	1.613	1.568	–	1.480	1.541
AlVI	–	0.356	0.343	–	0.446	0.472	–	0.390	0.311	–	0.449	0.436
Fe3+	–	0.694	0.666	–	0.028	0.339	–	0.685	0.606	–	0.043	0.133
Fe2+	0.010	1.430	1.454	0.032	2.621	2.277	0.000	1.937	1.952	0.000	2.374	2.326
Mn	0.000	0.053	0.049	0.003	0.042	0.036	0.000	0.101	0.103	0.000	0.067	0.061
Mg	0.000	2.269	2.294	0.007	1.606	1.649	0.020	1.721	1.846	0.000	1.814	1.826
Ca	0.400	1.775	1.812	0.372	1.882	1.797	0.340	1.833	1.881	0.330	1.797	1.825
Natot	0.560	0.366	0.342	0.593	0.294	0.341	0.670	0.291	0.279	0.670	0.539	0.549
Na(M4)	–	0.225	0.188	–	0.118	0.203	–	0.167	0.119	–	0.203	0.175
NaA	–	0.141	0.154	–	0.177	0.138	–	0.123	0.160	–	0.336	0.375
K	0.030	0.256	0.260	0.032	0.373	0.423	–	0.249	0.245	0.020	0.351	0.336
Fetot/(Fetot + Mg)	–	0.483	0.480	–	0.622	0.613	–	0.604	0.581	–	0.571	0.574
Anorthite	40.0	–	–	36.0	–	–	32.5			32.2	–	–
Albite	56.0	–	–	57.1	–	–	65.5			65.6	–	–
Orthoclase	3.2	–	–	3.0	–	–	–			1.7	–	–

Number of cations recalculated for plagioclase and amphibole on the basis of 8 and 13 oxygens, respectively. c = core, r = rim, Tsch: tschermakite, Fe-Tsch: ferrotschermakite, Ed: edenite, Fe-Ed: ferroedenite, Fe-Prg: ferropargasite.

maximum (Fig. 6). Since quartz is undeformed (or weakly deformed) and does not show an evident shape preferred orientation (SPO), the CPO likely reflects synmagmatic oriented grain growth in a direction favourable for prism-[c] slip (Gapais and Barbarin, 1986), and prism < a > slip.

Microfabric types (II) and (III) show similar c-axis fabric (Fig. 6), with some prominent near-X maxima, associated with secondary maxima located near the foliation poles (near-Z maxima). Such a fabric reflects intracrystalline deformation under a bulk non-coaxial flow regime, with the operation of prism-[c] slip (Mainprice et al., 1986) in cooperation with basal-<a> slip. The lack of near-Y maxima suggests that the inherited CPO from type (I) microfabric is likely small. Near-X maxima are stronger in quartz-rich leucogranites (samples Z5 and Z101.1), whereas the fabric within the quartz-poor Opx-bearing tonalite (e.g. samples SL1 and Z57) is markedly weaker and more diffuse, possibly reflecting variations in quartz content (Lisle, 1985). As a whole, the external symmetry of the CPO patterns is contradictory, indicating a dominant sinistral shear sense in four samples and dextral shear sense in two samples. However, the small number of grains measured some samples and their large size make the position of maxima in the pole figures somewhat unreliable as shear sense indicators. The determination of the shear sense prevailing during magmatic flow would require the examination of a more extensive and statistically-valid dataset.

Table 2
Average P-T estimates for selected DGS samples. The reported values represent average estimates for each sample. Errors for pressure and temperatures are taken from Anderson and Smith (1995) and Holland and Blundy (1994), respectively.

Sample	Magmatic assemblage	P (±0,6 kb)	T(±40 °C)
SSL2	Cpx-Opx-Hbl-Bt-Pl-Qtz	5,6	730
Z 79b	Cpx-Hbl-Bt-Pl-Qtz	5,4	720
Z 200	Cpx-Hbl-Bt-Pl-Qtz	5,5	709
Z 4	Hbl-Bt-Pl-Qtz	5,4	713

5.2. High-temperature solid-state fabric

Four end member CPO fabrics (referred here as SS1 to SS4 fabric) occur in the fifteen samples collected from high-temperature shear zones (Fig. 6). Since quartz is commonly completely recrystallized,

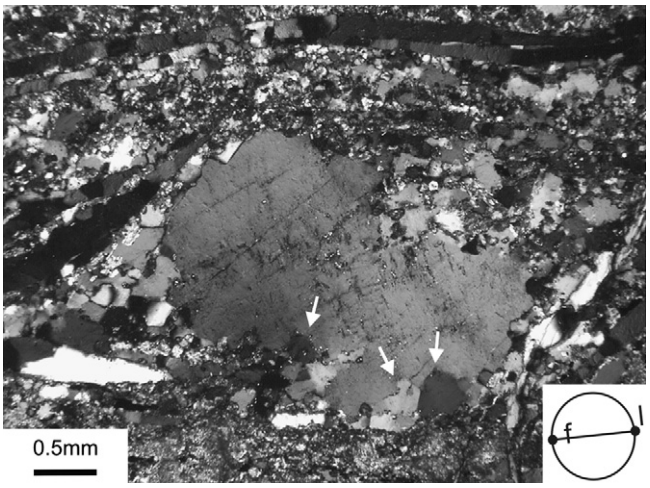

Fig. 5. Typical high-temperature microfabric from a sheared leucogranite, showing straight quartz ribbons alternating with layers of recrystallized feldspars (~100–300 μ in size), wrapping around feldspar porphyroclasts. Arrows indicate some subgrains at the periphery of the host K-feldspar (crossed polars).

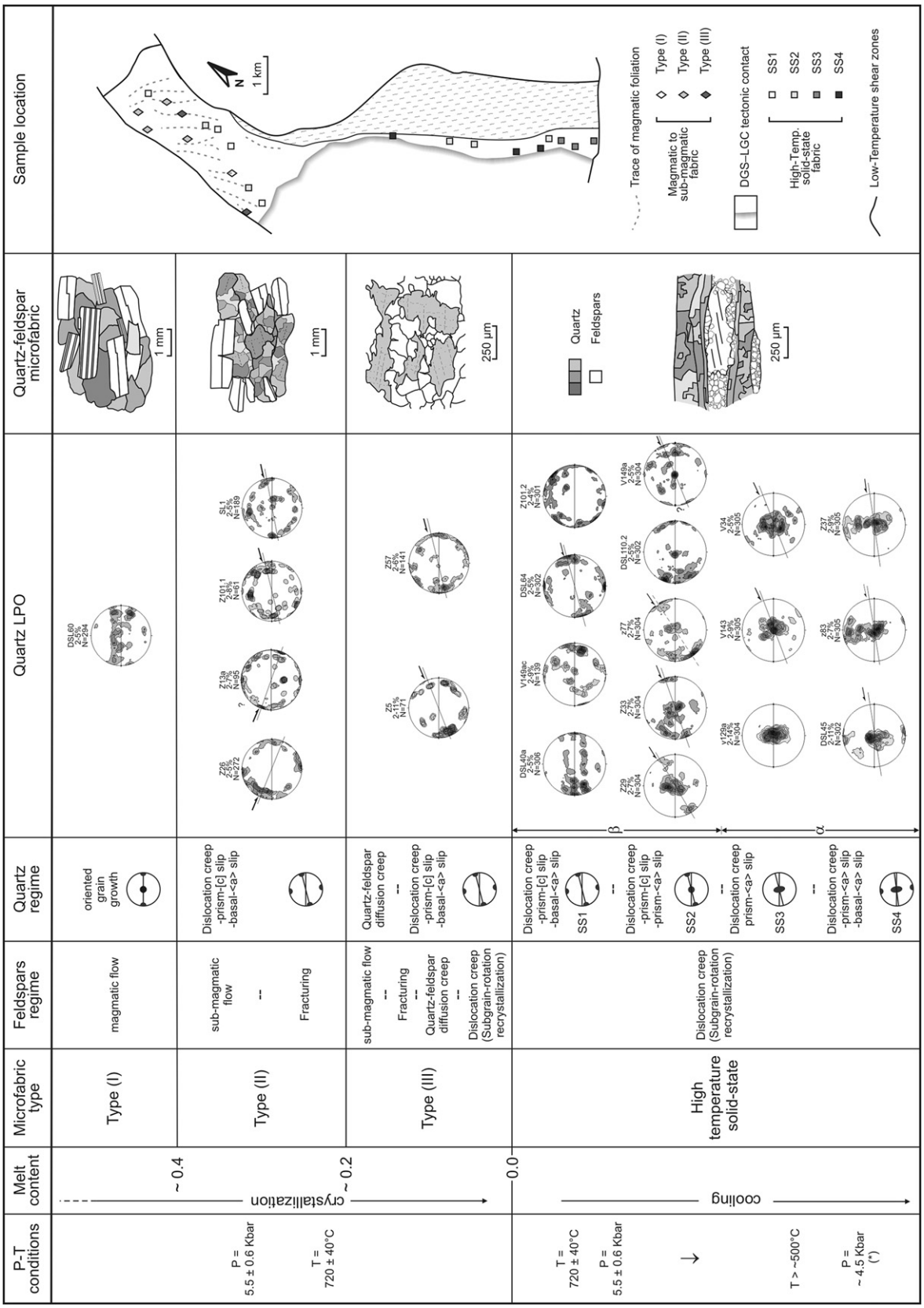

Fig. 6. Sketch illustrating the evolution of quartz c-axis fabrics during the transition from magmatic to solid-state flow. For each equal area stereographic projection (lower hemisphere, 1% of search area), the labels are (from top to bottom): sample name, contour interval (multiples uniform distribution) and number of measurements. All the analysed quartz grains from HT shear zones are recrystallized grains. Where possible, the shear plane (dotted line) and the inferred shear sense (half arrow) are indicated, as inferred from the external asymmetry of the patterns with respect to foliation and lineation (Bouchez et al., 1983). (*) Pressure estimation is after Thompson and England (1984), from the corresponding temperature inferred by microstructural criteria.

the inherited fabric from the magmatic stage is likely negligible. In sample DSL40a, SS1 fabric is analogous to the fabric developed under melt-present conditions, displaying a prominent near-X maximum associated with some secondary maxima symmetrically arranged along the XY plane, but without a near-Y maximum. Microfabric from three other narrow shear zones display a combination of near-X and near-Z maxima, in analogy of the CPO fabric typifying type (II) and (III) microfabric. SS2 CPO fabric display a combination of near-X and near-Y maxima, with a clear external symmetry indicating sinistral shear sense in three samples, whereas samples DSL110.2 and V149a display a nearly orthorhombic symmetry, consistently with the lack of shear sense indicators at thin section scale. SS3 CPO fabric displays a prominent near-Y maximum and lacks any near-X maxima. SS4 differs from SS3 by displaying a tendency towards a single girdle orthogonal to the mylonitic foliation, reflecting the onset of the subsequent greenschist facies retrograde evolution near the tectonic contact with the LGC (Zibra et al., 2010).

As a whole, these data suggest that a fabric transition occurred during the high-temperature solid-state flow. In the northern area, the microstructures and quartz CPOs may represent an incipient stage of shearing (see sample map in Fig. 6), at analogous PT conditions characterizing the magmatic stage, with evidence of dominant prism-[c] slip. These data also imply that a nearly identical quartz CPO fabric (compare samples DSL60 and DSL40a, Fig.6) may develop through different grain-scale mechanisms (i.e. oriented grain growth and dislocation creep, respectively).

Solid-state shearing continued in the low-quartz field, as testified by the dominant quartz CPO fabric preserved in the southern area (Fig. 6), where prism-<a> slip was prevailing, and prism-[c] slip was deactivated. Such a pattern represents the typical quartz fabric acquired at medium amphibolite-facies condition (Schmid and Casey, 1986), consistently with the observed microstructures (Zibra et al., 2010).

6. Discussion and conclusions

6.1. Relationship between DGS and SLSZ

Our systematic structural mapping testifies that, in the DGS, both magmatic and solid-state structures are markedly parallel to granulite-facies foliation and lineation in the SLSZ (Figs. 1 and 7). Moreover, sinistral shear sense dominated in both complexes during solid-state flow (see also Zibra et al., 2010), and it was probably prevailing even during hypersolidus flow in the DGS (Fig. 6). These data imply that the magmatic fabric pattern within the pluton likely reflects strain of magma caused by regional deformation rather than internal processes related to the construction of the magma chamber (Paterson et al., 1998). Accordingly, the occurrence of internal sheeting and compositional zoning at various scales suggests that the DGS was formed by multiple magma pulses during shearing (Neves et al., 1996; Paterson et al., 1998). Zibra et al. (2010) have shown that the main shear event along the SLSZ started at 286 ± 1 Ma (Paquette et al., 2003; M_1, Fig. 3) and ended at the depth of emplacement of the DGS (at 280 ± 2 Ma, Paquette et al., 2003; M_2, Fig. 3). These data provide independent evidence that shear deformation started before DGS emplacement, and it is therefore likely that the magma rose along the pre-existing and active shear zone. However, the former melt-channel is not exposed in the study area.

6.2. The evolution of microfabric during pluton crystallization

The data presented here suggest that the DGS recorded a continuous transition from magmatic to solid-state deformation. Coherent, continuous deformation during cooling is favoured for plutons emplaced at relatively deep crustal levels, where the pluton cools slowly enough (Paterson and Tobisch, 1988; Miller and Paterson, 1994). The prevailing tonalite composition may have facilitated the preservation of the transient microstructures developed during magma crystallization (Bouchez et al., 1992).

Figs. 6 and 7 illustrate the spatial distribution of different microfabrics within the DGS, and their geometric relationships with respect to the SLSZ. Microfabric type (I) corresponds to the "magmatic fabric s s" described elsewhere (e.g. Paterson et al., 1989; Vernon, 2000), where little or no grain-scale brittle and/or plastic deformation is visible. Our data show that, in absence of any important dislocation creep process, quartz may develop a clear CPO through oriented grain growth in a direction favourable for prism-[c] slip (Gapais and Barbarin, 1986), and for prism-<a> slip. However, as only one sample has been analysed, the role of type (I) CPO (as inherited fabric) during subsequent fabric evolution needs further investigations. In addition, the process of oriented grain growth might have played a role as a fabric-forming mechanism in the microstructure of microfabric (II) and (III) as well, as both developed under melt-present conditions. Microfabric type (II) is characterised by the occurrence of dominant prism-[c] slip, suggesting that dislocation creep process in quartz is not restricted to solid-state conditions, but may occur even during flow at melt fractions below ~0.4 (Rosenberg, 2001). The cuspate quartz-feldspar phase boundaries characterising microfabric type (III) has already been identified in amphibolite- (Gower and Simpson, 1992) and granulite-facies (Martelat et al., 1999) granitic gneiss deformed under solid-state conditions. Diffusion creep was also inferred to operate during experimental deformation of aplite under hypersolidus conditions ("melt-assisted diffusion creep", Dell'Angelo and Tullis, 1988), but only for very small grain size (~10 μm), as flow laws for Nabarro-Herring or Coble creep show that strain rate for diffusion creep has a marked grain size sensitivity (Poirier, 1985). Our most prominent result is that phase boundary migration assisted by diffusion creep may represent an important deformation mechanism even during hypersolidus flow in medium-grained quartzofeldspathic aggregates. On the other hand, experiments have shown that the occurrence of melt along grain boundaries can markedly enhance diffusion rates, allowing diffusion creep to operate in coarse-grained aggregates (Tullis and Yund, 1991).

Microfabric types (II) and (III) are associated with magmatic microfractures, which might reflect an increase in the solid fraction in the crystal mush. As only a few fractured grains per thin section commonly occur, brittle deformation probably did not represent the dominant deformation mechanism in our samples However, the occurrence of microfractures testifies that, during pluton crystallisation, diffusion creep, dislocation creep and grain-scale fracturing cooperated in accommodating the deformation in the partially molten quartzofeldspathic aggregate.

Estimation of melt content during the development of each microfabric is not straightforward, as the influence of strain rate, crystal shape (Kerr and Lister, 1991) and magma composition (Bouchez et al., 1992) on magma rheology is still poorly understood. The strain rate likely plays a dominant role in controlling the microstructure. Assuming that the melt phase is non-Newtonian and the crystals are not elastic (Bagdassarov and Dorfman, 1998), low-strain rates will favour the preservation of type (I) microfabric even during flow at very low melt fractions (Rosenberg, 2001). The onset of synmagmatic brittle deformation may approximately correspond to the transition from suspension flow to grain-supported flow, which is thought to occur in deforming magmas at melt fractions of ~0.4–0.2 ("solid to liquid transition", SLT, Rosenberg and Handy, 2005). Therefore, in absence of any

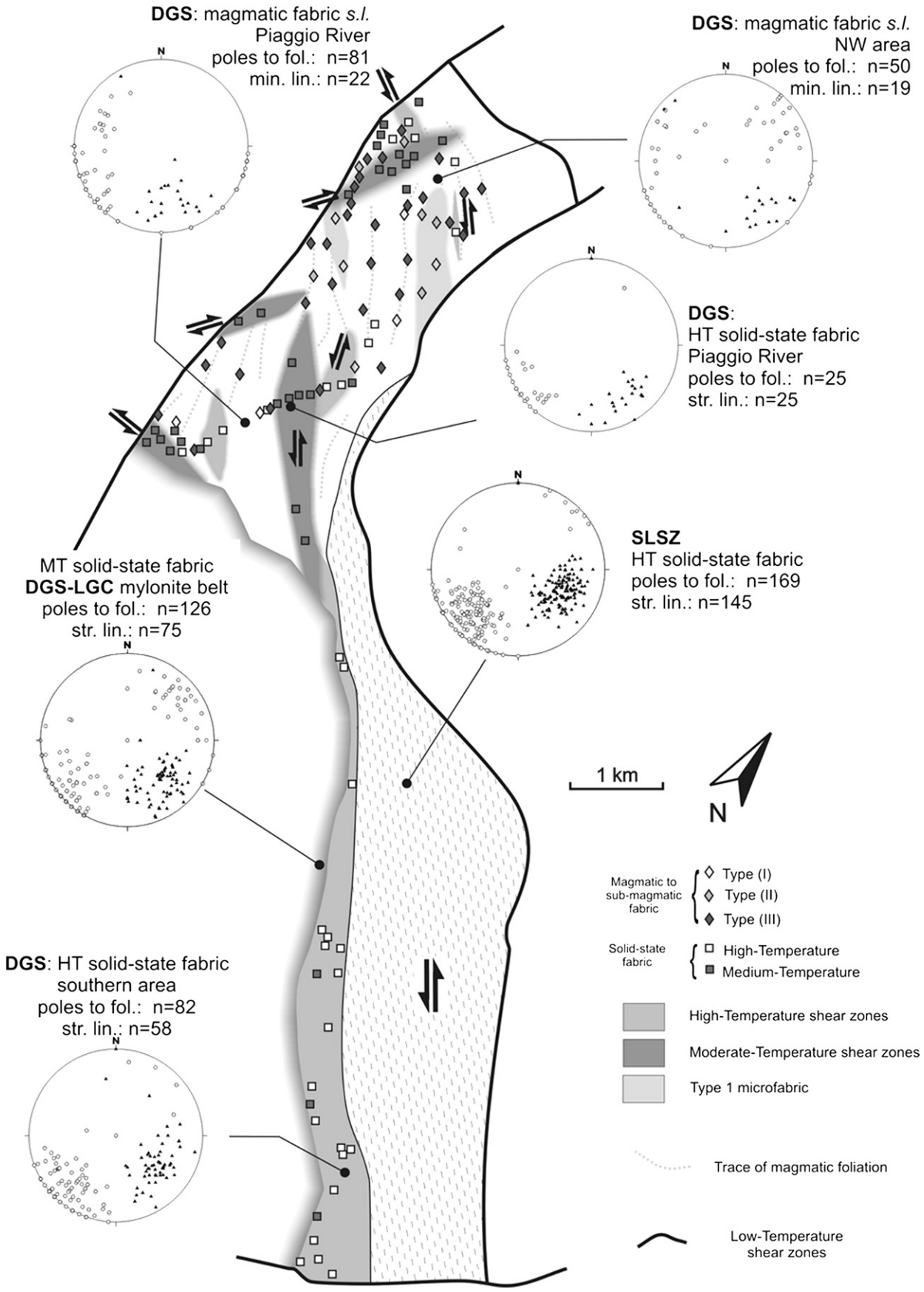

Fig. 7. Spatial distribution of different microfabrics within the DGS, with insets of equal area projection plots (lower hemisphere) of mineral and stretching lineation (black triangles) and poles to foliation (open circles). Dashed lines in the northern area indicate the trace of the hypersolidus foliation.

independent data about strain rate, we postulate that microfabric types (II) and (III) developed during pluton crystallization at melt fractions ~ 0.4–0.0. Definitions like "submagmatic flow" and "flow at low melt fraction" (Rosenberg, 2001) both fit with microstructures observed in our samples. Hypersolidus structures are cut by narrow shear zones, developed at near-solidus temperature, providing the transition to solid-state flow under a consistent kinematic framework. This transition corresponds to a drastic change from distributed to markedly localized flow. Therefore, we suggest that in our case study the transition from homogeneous to heterogeneous flow is not related to a switch in the dominant deformation mechanisms and dramatic grain size reduction during cooling (Gapais and Barbarin, 1986), as quartz and feldspar behaviour did not change substantially during the latest stages of pluton crystallization (Fig. 6), but it could be controlled by the occurrence of interstitial melt in the aggregate. Accordingly, experiments show that a drastic strain hardening is expected during the very last stages of crystallization, at melt fraction as low as 0.07 ("Melt connectivity transition", MCT, Rosenberg and Handy, 2005). There is also evidence that a dramatic change in viscosity occurs even during natural deformation, as theoretically derived flow laws for melt-bearing granite show that the viscosity increases most strongly at very low melt volumes (3–5%, Rosenberg et al., 2007). The microstructural map (Fig.7) also shows that type (III) microfabric occurs in 70% of our samples, whereas samples with types (I) and (II) are mainly found within a few low-strain, lozenge-shaped domains. Consistently with field observations (primary foliation overprinting igneous contacts), these data suggest that emplacement occurred at melt fractions higher than ~0.40, and that the observed hypersolidus fabrics formed after pluton emplacement, reflecting the stress field imposed by the SLSZ, and preserving no memory of the ascent stage.

Acknowledgements

We thank S. R. Paterson and H. Stünitz for their constructive and detailed reviews. The stimulating discussions with Claudio Rosenberg and Giancarlo Molli significantly improved the quality of this paper. Their frequent encouragements are gratefully acknowledged. Murray Jones and Michael Prause are thanked for improving the quality of some figures. Quartz *c*-axis determinations were carried out on a Futron™ semi-automated universal stage at the Tectonics and Material Fabrics Section, Technische Universität München.

References

Anderson, J.L., 1996. Status of thermo barometry in granitic batholiths. Transactions of the Royal Society of Edinburgh: Earth Sciences 87, 125–138.
Anderson, J.L., Smith, D.R., 1995. The effects of temperature and f_{o2} on the Al-in-hornblende barometer. American Mineralogist 80, 549–559.
Bagdassarov, N., Dorfman, A., 1998. Granite rheology: magma flow and melt migration. Journal of the Geological Society of London 155, 863–872.
Blumenfeld, P., Bouchez, J.L., 1988. Shear criteria in granite and migmatite deformed in the magmatic and solid states. Journal of Structural Geology 10, 361–372.
Bodorkos, S., Cawood, P.A., Oliver, N.H.S., 2000. Timing and duration of syn-magmatic deformation in the Mabel Downs Tonalite, northern Australia. Journal of Structural Geology 22, 1181–1198.
Bouchez, J.L., Lister, G.S., Nicolas, A., 1983. Fabric asymmetry and shear sense in movement zones. Geologische Rundschau 72, 401–419.
Bouchez, J.L., Delas, C., Gleizes, G., Nedelec, A., Cuney, M., 1992. Submagmatic microfractures in granites. Geology 20, 35–38.
Büttner, S.H., 1999. The geometric evolution of structures in granite during continuous deformation from magmatic to solid-state conditions: an example from the central European Variscan belt. American Mineralogist 84, 1781–1792.
Caron, J.M., 1994. Metamorphism and deformation in alpine Corsica. Schweizerische Mineralogische und Petrographische Mitteilungen 74, 105–114.
Clemens, J.D., Wall, V.J., 1981. Origin and crystallization of some peraluminous (S-type) granitic magmas. Canadian Mineralogist 19, 111–131.
Dell'Angelo, L.N., Tullis, J., 1988. Experimental deformation of partially melted granitic aggregates. Journal of Metamorphic Geology 6, 495–515.
Doglioni, C., Gueguen, E., Sàbat, F., Fernandez, M., 1997. The western Mediterranean extensional basins and the alpine orogen. Terra Nova 9, 109–112.
Egal, E., 1992. Structures and tectonic evolution of the external zone of Alpine Corsica. Journal of Structural Geology 14, 1215–1228.
Gapais, D., Barbarin, B., 1986. Quartz fabric transition in a cooling syntectonic granite (Hermitage Massif, France). Tectonophysics 125, 357–370.
Gower, R.J.W., Simpson, C., 1992. Phase boundary mobility in naturally deformed, high-grade quartzofeldspathic rocks: evidence for diffusional creep. Journal of Structural Geology 14, 301–314.
Gross, A.F.K., Van Heege, J.P.T., 1973. The high-low quartz transition up to 10 Kb pressure. Journal of Geology 81, 717–724.
Holland, T., Blundy, J., 1994. Non-ideal interactions in calcic amphiboles and their bearing on amphibole–plagioclase thermometry. Contributions to Mineralogy and Petrology 116, 433–447.
Hutton, H.W., 1988. Granite emplacement mechanisms and tectonic controls: inferences from deformation studies. Transactions of the Royal Society of Edinburgh: Earth Sciences 79, 245–255.
Ji, S., Mainprice, D., 1990. Recrystallization and fabric development in plagioclase. Journal of Geology 98, 65–79.
Johannes, W., 1984. Beginning of melting in the granite system Qz-Or-Ab-An-H2O. Contributions to Mineralogy and Petrology 86, 264–273.
John, B.E., Stünitz, H., 1997. Magmatic fracturing and small-scale melt segregation during pluton emplacement: evidence from the Adamello massif (Italy). In: Bouchez, J.L., Hutton, D.H.W., Stephens, W.E. (Eds.), Granite: From Segregation of Melt to Emplacement Fabrics. Kluwer, Dordrecht, pp. 55–74.
Karlstrom, K.E., Miller, C.F., Kingsbury, J.A., Wooden, J.L., 1993. Pluton emplacement along an active ductile thrust zone, Piute Mountains, Southeastern California: interaction between deformational and solidification processes. Geological Society of America Bulletin 105, 213–230.
Kerr, R.C., Lister, J.R., 1991. The effects of shape on crystal settling and on the rheology of magmas. Journal of Geology 99, 457–467.
Kruhl, J.H., 1996. Prism and basal-plane parallel subgrain boundaries in quartz: a microstructural geothermobarometer. Journal of Metamorphic Geology 14, 581–589.
Leake, B.E., 1997. Nomenclature of amphiboles report of the subcommitee on amphiboles of the International Mineralogical Commission on New minerals and mineral Names. European Journal of Mineralogy 9, 623–651.
Libourel, G., 1985. Le complexe de Santa Lucia di Mercurio (Corse). Ph.D. Thesis, Toulouse University (France).
Lisle, R.J., 1985. The effect of composition and strain on quartz –fabric intensity in pebbles from a deformed conglomerate. Geologische Rundschau 74, 657–663.
Mainprice, D.H., Bouchez, J.L., Blumenfeld, P., Tubia, J.M., 1986. Dominant c slip in naturally deformed quartz: implications for dramatic plastic softening at high temperature. Geology 14, 819–822.
Martelat, J.E., Schulmann, K., Lardeaux, J.M., Nicollet, C., Cardon, H., 1999. Granulite microfabrics and deformation mechanisms in southern Madagascar. Journal of Structural Geology 21, 671–688.
Miller, R.B., Paterson, S.R., 1994. The transition from magmatic to high-temperature solid-state deformation: implications from the Mount Stuart batholith, Washington. Journal of Structural Geology 16, 853–865.
Neves, S.P., Vauchez, A., Archanjo, C.J., 1996. Shear zone-controlled magma emplacement or magma-assisted nucleation of shear zones? Insights from northeast Brazil. Tectonophysics 262, 349–364.
Paquette, J.L., Ménot, R.P., Pin, C., Orsini, J.P., 2003. Episodic and short-lived granitic pulses in a post-collisional setting: evidence from precise U-Pb zircon dating through a crustal cross-section in Corsica. Chemical Geology 198, 1–20.
Passchier, C.W., Trouw, R.A.J., 2005. Microtectonics, second ed. Springer, Berlin, Heidelberg, New York.
Paterson, S.R., Schmidt, K.L., 1999. Is there a close spatial relationship between faults and plutons? Journal of Structural Geology 21, 1131–1142.
Paterson, S.R., Tobisch, O.T., 1988. Using pluton ages to determine regional deformations: problems with commonly used criteria. Geology 16, 1108–1111.
Paterson, S.R., Tobisch, O.T., 1992. Rates of processes in magmatic arcs: implications for the timing and nature of pluton emplacement and wall rock deformation. Journal of Structural Geology 14, 291–300.
Paterson, S.R., Vernon, R.H., Tobisch, O.T., 1989. A review of criteria for the identifications of magmatic and tectonic foliations in granitoids. Journal of Structural Geology 11, 349–363.
Paterson, S.R., Fowler Jr., T.K., Schmidt, K.L., Yoshinobu, A.S., Yuan, E.S., Miller, R.B., 1998. Interpreting magmatic fabric patterns in plutons. Lithos 44, 53–82.
Petford, N., Cruden, A.R., McCaffrey, K.J.W., Vigneresse, J.L., 2000. Granite magma formation, transport and emplacement in the Earth's crust. Nature 408, 669–673.
Poirier, J.P., 1985. Creep of Crystals: High-temperature Deformation Processes in Metals, Ceramics and Minerals. Cambridge University press, Cambridge.
Rosenberg, C.L., 2001. Deformation of partially molten granite: a review and comparison of experimental and natural case studies. International Journal of Earth Sciences 90, 60–76.
Rosenberg, C.L., 2004. Shear zones and magma ascent: a model based on a review of the Tertiary magmatism in the Alps. Tectonics 23, 1–21.

Rosenberg, C.L., Handy, M.R., 2005. Experimental deformation of partially melted granite revisited: implications for the continental crust. Journal of Metamorphic Geology 23, 19–28.
Rosenberg, C.L., Stünitz, H., 2003. Deformation and recrystallization of plagioclase along a temperature gradient: an example from the Bergell tonalite. Journal of Structural Geology 25, 389–408.
Rosenberg, C.L., Medvedev, S., Handy, M., 2007. On the effects of melting on continental deformation and faulting. In: Handy, M., Hirth, G., Hovius, N. (Eds.), Tectonic Faults: Agents of Change on a Dynamic Earth. M.I.T. Press, pp. 357–402.
Rossi, P., Cocherie, A., Fanning, C.M., Deloule, E., 2005. Variscan to Eo-alpine events recorded in European lower-crust zircons sampled from the French massif central and Corsica, France. Lithos 87, 235–260.
Schmid, S.M., Casey, M., 1986. Complete fabric analysis of some commonly observed quartz c-axis patterns. Geophysical Monograph 36, 263–286.
Singh, J., Johannes, W., 1996. Dehydration melting of tonalites. Part I: Beginning of melting. Contributions to Mineralogy and Petrology 125, 16–25.
Stipp, M., Stünitz, H., Heilbronner, R., Schmid, S.M., 2002. The eastern Tonale fault zone: a "natural laboratory" for crystal plastic deformation of quartz over a temperature range of 250 to 700°C. Journal of Structural Geology 24, 1861–1884.
Thompson, A.B., England, P.C., 1984. Pressure-temperature-time paths of regional metamorphism. II. Their inference and interpretation using mineral assemblages in metamorphic rocks. Journal of Petrology 25, 929–955.
Tullis, J., Yund, R.A., 1991. Experimental evidence for diffusion creep in feldspar aggregates. Journal of Structural Geology 13, 987–1000.
Vernon, R.H., 2000. Review of microstructural evidence of magmatic and solid-state flow. Electronic Geosciences 5, 2.
Vielzeuf, D., Montel, J.M., 1994. Partial melting of metagreywackes. 1. Fluid-absent experiments and phase relationships. Contributions to Mineralogy and Petrology 117, 375–393.
Vielzeuf, D., Schmidt, M.W., 2001. Melting relations in hydrous systems revisited: application to metapelites, metagreywackes and metabasalts. Contributions to Mineralogy and Petrology 141, 251–267.
Zibra, I., 2006. Late-Hercynian granitoid plutons emplaced along a deep crustal shear zone. A case study from the S. Lucia Nappe (Alpine Corsica, France). Ph.D. Thesis, Pisa University (Italy). The complete manuscript is Available from: http://etd.adm.unipi.it/theses/available/etd-09142006-171856/.
Zibra, I., Kruhl, J.H., Braga, R., 2010. Late Palaeozoic deformation of post-Variscan lower crust: shear zone widening due to strain localization during retrograde shearing. International Journal of Earth Sciences 99, 973–991.